N O T I C E

THIS DOCUMENT HAS BEEN REPRODUCED FROM MICROFICHE. ALTHOUGH IT IS RECOGNIZED THAT CERTAIN PORTIONS ARE ILLEGIBLE, IT IS BEING RELEASED IN THE INTEREST OF MAKING AVAILABLE AS MUCH INFORMATION AS POSSIBLE

U. of Iowa 80-6

Particle Energization in the Inner, Nonazimuthally Symmetric Magnetospheres of Neutron Stars

by

JOSEPH E. BOROVSKY,[1] CHRISTOPH K. GOERTZ,[2]

and GLENN JOYCE[3]

Department of Physics and Astronomy
The University of Iowa
Iowa City, Iowa 52242

March 1980

[1] Presently at NASA/Goddard Space Flight Center, Planetary Magnetospheres Branch, Greenbelt, Maryland 20771.

[2] Presently at Max-Planck Institut für Aeronomy, Postfach 20, D-3411 Katlenburg, Lindau 3, West Germany.

[3] Presently at JAYCOR, 205 South Whiting Street, Alexandria, Virginia 22304.

ABSTRACT

The energization process of magnetic pumping, a combination of time-dependent magnetic mirror fields with pitch-angle scattering, is applied to trapped charged particles $\vec{E} \times \vec{B}$ drifting in corotating, azimuthally nonsymmetric neutron star magnetospheres. When particle energization is balanced by synchrotron radiation loss, it is found that protons, rather than electrons, reach considerable kinetic energies and radiate, in the x-ray regime, at rates up to the 10^6 MeV/proton/sec.

Subject headings: plasma processes — x-ray binaries — magnetospheres — neutron stars

I. INTRODUCTION

Several compact x-ray sources are known to be members of close binary systems (Gurskey and Schreir 1975). We propose that the environment of a magnetized neutron star in a close binary system is favorable for the energization, by the process of magnetic pumping, of the magnetospheric charged particles, and that these particles will be capable of emitting, with considerable power, synchrotron radiation in the x-ray region of the spectrum.

The magnetic-pumping mechanism for the energization of charged particles in magnetic-mirror geometries was first proposed by Alfvén (1954). In his simple model, described in Alfvén and Fälthammar (1963, Sect. 2.7.4), cyclic variations of the magnetic field strength are combined with isotropization of the particle distribution functions when the field strength reaches a maximum or a minimum. As the field strength is increased, the mean perpendicular (to $\vec{B}$) momentum of the distribution increases, conserving the first adiabatic invariant of each particle, while the mean parallel momentum remains constant. Isotropization when the field is at a maximum turns some of the high perpendicular momenta of the distribution into high parallel momenta, which do not decrease with the decreasing of the magnetic field. This leads to an increase in the mean

momentum of the distribution with time. In the Alfvénic model, the momentum after one cycle is given by

$$P = P_o \frac{1}{3}\left[5 + 2k + 2/k\right]^{1/2} \quad , \tag{1}$$

where P_o is the initial momentum and k is the magnetic ratio of the cycle,

$$k = B_{o_{MAX}}/B_{o_{MIN}} \quad , \tag{2}$$

the B_o values being the field strength in the magnetic mirror mid-plane (equatorial region for magnetospheres). Equation (1) results in a variation in time for the mean momentum, if the magnetic pumping is not balanced by another mechanism, which is of the form

$$P = P_o e^{t/\tau_E} \quad , \tag{3}$$

where τ_E is defined as an energization time.

More realistic, but not simple to solve, is the case of pitch-angle (momentum-conserving) scattering of particles occurring constantly as the magnetic field varies, in contrast to the infinite pitch-angle diffusion imposed at times of magnetic field maxima and

minima in the Alfvén model. In order to solve this problem, we have developed formalisms to follow the adiabatic motions of particles in the magnetic-mirror topology of an asymmetric magnetosphere and to solve a diffusion equation representing the pitch-angle scattering of particles.

As the magnetic field varies we numerically follow, in momentum-pitch-angle phase space, the evolution of $n(p,\alpha_o)$, the number of particles in a flux tube with momentum p and equatorial (at the mirror midplane) pitch-angle α_o, calculating the new phase-space coordinates. In our relativistic treatment, particle motion conserves the first adiabatic invariant

$$\mu = p_\perp^2/B \tag{4}$$

(no longer the magnetic moment), the total energy

$$E = \gamma\, mc^2 \pm eV \quad , \tag{5}$$

and the second adiabatic invariant

$$J = \oint p_\parallel \, ds \quad , \tag{6}$$

where $\perp$ and $\parallel$ are with respect to the magnetic field, V is an electric potential, and γ is the relativistic factor $(1 - V^2/c^2)^{-1/2}$. In order to simplify the treatment, a special shape for the magnetic-mirror field is chosen (Goertz 1978; Borovsky et al. 1980), with the magnetic-pumping results found to be quite insensitive to the choice of magnetic field topology. For a more detailed discussion we refer the reader to the paper by Borovsky et al. (1980) where a similar mechanism was applied to the case of Jupiter.

In order to describe the diffusion, caused by particle scattering in the distribution, in pitch-angle space, we solve the "bounce-averaged" Fokker-Planck equation

$$\frac{\partial n}{\partial t} = \frac{\partial}{\partial \alpha_o} \left[T(\alpha_o) \sin \alpha_o \cos \alpha_o \, \mathcal{D}(\alpha_o) \frac{\partial}{\partial \alpha_o} \right.$$
$$\left. \times \left\{ n(\alpha_o)/T(\alpha_o) \sin \alpha_o \cos \alpha_o \right\} \right] \quad , \tag{7}$$

where $T(\alpha_o)$ is the angular dependence of a particle bounce period and $\mathcal{D}(\alpha_o)$ is the "bounce-averaged" diffusion coefficient. Bounce averaging allows the description of off-equatorial (away from the midplane) scattering in terms of equatorial parameters. The time asymptotic solution to the diffusion equation is an isotropic distribution function $f(\alpha_o)$ = constant, where $f(\alpha_o)$ and $n(\alpha_o)$ are related by

$$f(\alpha_o) = n(\alpha_o)/T(\alpha_o)\sin \alpha_o \cos \alpha_o \quad . \tag{8}$$

Combining the adiabatic motion with the pitch-angle scattering allows us to simulate magnetic-pumping processes. For the numerical procedure chosen, it is easily shown that alternately solving for the adiabatic motion and for the pitch-angle diffusion is equivalent to solving the Boltzmann equation for particles undergoing the magnetic-pumping process. In conforming our simulation parameters to the special case of the Alfvén model, we find very satisfactory agreement between our results and analytical theory.

II. THE MAGNETIC FIELD

The model magnetic field chosen is a rotationally aligned (magnetic moment parallel to angular momentum) dipole with a slight compression (increase) on one side. The equatorial field strength on the dipolar (noncompressed) side is given by

$$B_D = \frac{M}{r^3} \quad , \tag{9}$$

where M is the magnetic dipole moment. For the form of the compressed-dipole side, we choose

$$B_c = \frac{M}{r^3} + \frac{M'}{r^2} \quad . \tag{10}$$

A measure of the magnetic field distortion is r_{COMP}, the radius where the compression amounts to a 10% increase in the equatorial field strength, i.e.,

$$B_c = 1.1\, B_D \quad \text{at} \quad r = r_{COMP} \quad , \tag{11}$$

yielding, from (10),

$$M' r_{COMP} = \frac{1}{10} M \quad . \tag{12}$$

Thus, the values of M and r_{COMP} will define a value for M'.

We assume that the potentials in the inner magnetosphere arise from corotational electric fields (we discuss corotation below) and we will require that the potentials of both sides be equal at the stellar surface, $r = r_s$. On the dipolar side we have (by integrating $E = 1/c\ \vec{v} \times \vec{B}_D$),

$$V_D = \frac{\Omega}{c} \frac{M}{r} \quad , \tag{13}$$

where Ω is the angular frequency of stellar rotation, and on the compressed side we have

$$V_c = \frac{\Omega}{c} \left[\frac{M}{r} + M' \log\left(\frac{r_s}{r}\right) \right] \quad , \tag{14}$$

which is equal to V_D at $r = r_s$.

The adiabatic motion of charged particles conserves (Equations (4), (5), and (6)) the first adiabatic invariant μ, the second adiabatic invariant J, and the total energy E. For particles

with much less kinetic energy than potential energy, the drift orbits will lie almost exactly on equipotential surfaces and the particles will drift through regions of differing magnetic field strength. (The violation of this will provide a limit for the energization process, discussed below.) Since we know the magnetic fields $B(r)$ and potentials $V(r)$ on both sides of the star, we may calculate the ratio $k = B_{o_{MAX}}/B_{o_{MIN}}$ for particles in orbits following equipotentials. Hence, for choices of diffusion coefficients (see below), we may calculate the magnetic-pumping energization times, τ_E, as functions of radius.

We estimate, for the parameters of our model, the regions of the magnetosphere in which the model will be plausible. We take the (neutron) stellar radius to be 10 kilometers ($r_s = 10^6$ cm). This will be the inner limit for the validity of the model. We do not expect corotation of the magnetosphere out to the light cylinder (radius at which the corotational velocity equals the velocity of light), which for our rotational period $\tau_{ROT} = 2$ sec, is $r_L = 95{,}500$ km $= 9.55 \times 10^9$ cm. Corotation might be expected (Lamb et al. 1973) to hold out to the distance where the corotational velocity is equal to the Kepplarian orbital velocity ($r > r_k \Rightarrow V_{COR} > V_{ORBIT}$). This Kepplarian radius is given by

$$r_k = \left(\frac{G\, m_s}{\Omega^2}\right)^{1/3} = 3480 \text{ km} \left(\frac{m_s}{m_\odot}\right)^{1/3} , \qquad (15)$$

where m_s is the stellar mass. For $m_s = 1\ m_\odot$ we find $r_k = 3480$ km and for $m_s = .1\ m_\odot$ we find $r_k = 1615$ km. A relativistic plasma theory for pulsar magnetospheres (Hinta and Jackson 1974) predicts the outer limit of corotation to be

$$r_{COR} = r_s^{3/5} \left(\frac{c}{\Omega}\right)^{2/5} = r_s^{3/5}\ r_L^{2/5} \quad , \tag{16}$$

which, for our model, is $r_{COR} = 391$ km $= 3.91 \times 10^7$ cm. At these limiting radii the corotational velocities are nonrelativistic ($r = 391$ km $\Rightarrow V_{COR} = c/250$ and $r = 300$ km $\Rightarrow V_{COR} = c/320$), so we may assume the particle drifts to be adiabatic, and in particular, may be confident that the second adiabatic invariant, $J = \oint P_{\|}\ ds$, is conserved.

As an agent for the pitch-angle scattering of the charged particles we assume the presence of plasma waves, excited by anisotropic particle distributions produced by the adiabatic motion. In calculating the energization times as functions of the equatorial distance from the star (k(r)known), we use the continuous diffusion model and assume that the mechanism runs at its optimum diffusion rate ($\tau_{DIF}/\tau_{ROT} = 1$, where τ_{DIF} is the diffusion time and τ_{ROT} is the rotation period, see Borovsky, Chap. V; Borovsky et al. 1980). This choice is not critical since diffusion rates an order of magnitude above or below this value give energization times differing by at most, a factor of three.

III. RESULTS OF THE MODEL

We now have the information necessary for the construction of a model which energizes particles in the asymmetric magnetosphere. Without additional processes we would expect the energy of particles to increase indefinitely. There are, however, two phenomena which limit particle energy. The first is the condition that a particle have less kinetic energy than potential energy. If this requirement is met, a particle's drift orbit will approximate an electrical equipotential and the drift will carry the particle through regions of differing magnetic field strength, essential for the success of the energization process. If, instead, a particle's kinetic energy exceeds its potential energy, then the drift path will follow contours of equal magnetic field strength and no energization will occur ($k \rightarrow 1$). To estimate this kinetic-energy upper-limit, we calculate the difference in electrical potential, ΔV, along a contour of equal equatorial magnetic-field strength and require particle kinetic energies to be less than $e\,\Delta V$. Thus our limit appears as

$$(\gamma_L - 1)mc^2 = e\,\Delta V \quad , \tag{17}$$

where γ is the relativistic factor $(1 - v^2/c^2)^{-1/2}$ and the L subscript pertains to the value at the limit. This limiting kinetic energy appears (in terms of γ_L) in Figures 2 - 6 as the hollow circles.

But even when $\gamma < \gamma_L$ the energy does not necessarily increase because energy is lost through synchrotron radiation, the power radiated being approximately proportional to the square of the particle energy ($P \propto [\gamma^2 - 1]$). The fact that, in the synchrotron mode, the power radiated by a particle of set energy is proportional to the inverse-four power of the particle mass, and thus more effective for electrons than protons, leads to an important prediction of our model; that protons, not electrons, gain the energy and radiate it away. To find the limiting kinetic energy we will equate the energization time, τ_E, with the radiative lifetime for relativistic particles (Alfvén and Fälthammar 1963)

$$\tau_R = \frac{3\, c^5\, m^3}{2\, e^4} \frac{1}{B^2} \frac{1}{1 + \gamma_R} \quad . \tag{18}$$

Equating this to τ_E yields the relativistic factor γ as a function of the radius r (on the compressed side),

$$\gamma_R = \frac{3\, c^5\, m^3}{2\, e^4} \frac{1}{B^2} \frac{1}{\tau_E} - 1 \quad , \tag{19}$$

where B and τ_E are functions of r. This value appears as the solid circles in Figures 2 - 6. If, at a particular radius, the γ_R value obtained by balancing energization with radiative loss is lower than the γ_L value of the mechanism limit (kinetic less than potential), then γ_R will be the relativistic factor of the particle there, that is, particles are energized up to and maintained at the energy $E = \gamma_R\ mc^2$. If the value γ_L is lower than the value γ_R, the particles are energized to and maintained at the energy $E = \gamma_L\ mc^2$. The variation of γ is shown as the solid line in Figures 2 - 6, where γ is always the smaller of the two values, γ_R and γ_L.

Knowing the particle kinetic energies, $(\gamma - 1)mc^2$, and magnetic field strength, B, as functions of r, we may calculate the wavelength, λ_m, of the maximum synchrotron-radiated power as a function of r. With the frequency of the peak power being

$$\nu_m = \frac{1}{2\pi}\ \frac{eB}{mc}\ \gamma^2 \quad , \tag{20}$$

we have $(\lambda = c/\nu)$

$$\lambda_m = \frac{2\pi\, mc^2}{e}\ \frac{1}{B}\ \frac{1}{\gamma^2} \quad . \tag{21}$$

These wavelengths, for protons, appear in Figures 2 - 6 as solid squares for the radiation-limited proton energies $(\lambda_m(\gamma_R))$ and as

hollow squares for the mechanism-limited proton energies ($\lambda_m(\gamma_L)$), the solid curve taking the wavelengths pertaining to the characteristic (lesser of γ_R and γ_L) value. Electron radiation-limited wavelengths appear in these graphs as the solid triangles, but, due to the fact that rapid radiative loss limits them to low kinetic energies, the emission is strictly through the cyclotron mode.

We examine five cases (Figures 2 - 6), combinations of medium ($M = 5 \times 10^{28}$ gauss cm^3) or weak ($M = 5 \times 10^{27}$ gauss cm^3) magnetic dipole moments with weak (r_{COMP} = 955 km) or strong (r_{COMP} = 95.5 km) compressions and one of a strong ($M = 5 \times 10^{29}$ gauss cm^3) magnetic dipole with weak compression. In the weak dipole (meaning, also, weak corotational potentials) cases (Figures 2 and 5), the proton energies are more restricted by the (kinetic less than potential) mechanism limit, while, in the medium dipole cases (Figures 3 and 6), protons are energized at distances further from the star, in regions in which we are less confident in the application of our model. In the case of the medium dipole-weak compression (Figure 3), the energy limit dominates the radiative balance at r = 320 km (still within the Hinata and Jackson corotation limit, r_{COR}), where the characteristic wavelength of the synchrotron emission is 2.8×10^{-7} cm, in the weak x-ray region. For the case of the medium dipole-strong compression (Figure 6), mechanism-limiting occurs at a distance of r = 234 km, where the characteristic radiation is in the strong x-ray regime, $\lambda_m = 1.1 \times 10^{-9}$ cm. In a strong

dipole- ($M = 5 \times 10^{29}$ gauss cm^3; applicable to the Crab Nebula pulsar) weak compression (again, $r_{COMP} = 955$ km) case (Figure 4), we find a limited wavelength of 2.2×10^{-9} cm (strong x-ray region) at a distance $r = 730$ km, which, however, may not be in the corotating zone.

As a value for the power radiated per particle, we use the particle kinetic energy divided by its radiative lifetime,

$$P = \frac{(\gamma - 1)mc^2}{\tau_R} \quad , \tag{22}$$

where γ is the appropriate relativistic factor, γ_R or γ_L, and the lifetime τ_R is given by Equation (18) (using γ_R or γ_L). The power radiated per proton is displayed, for the four above cases, in Figure 7, where the substantial radiated-power prediction ($> 10^4$ MeV/sec/proton) of the model may be seen. It is important to realize that, in the cases studied, the power radiated by electrons is less by 10 or more orders of magnitude. This is due to the short radiative lifetimes of electrons which keep their kinetic energies (and momenta) low. The energy gain per unit time, and hence the energy radiated per unit time, is proportional to the particle kinetic energy (see Equation (3)), so the low-energy electrons gain little energy from the magnetic pumping, hence radiate little power.

We note that (for $\gamma \gg 1$) as the stellar rotation rate $\Omega = 2\pi \tau_{ROT}^{-1}$ increases, the radiation-limited γ-values, γ_R (Equation (19)), increase proportional to Ω, the characteristic synchrotron wavelengths, λ_m (Equation (21)), decrease proportional to Ω^{-2}, and the power radiated per particle, P (Equation (22)), increases proportional to Ω^2. We also note that, since the corotational electrical potentials (Equation (13)) are proportional to the angular rotation rate Ω, the mechanism-limiting γ-values, γ_L (Equation (17)), increase proportional to Ω as do the radiation-limited values, γ_R. Thus, if we increase the rotation rate of our model by a factor of $\sqrt{10}$ ($\Omega \rightarrow \sqrt{10}\ \Omega$ and $\tau_{ROT} = 2$ sec $\rightarrow \tau_{ROT} = .63$ sec), the characteristic wavelengths as functions of the radius will all decrease by a factor of 10 and the radiated power per particle will increase by a factor of 10.

IV. DISCUSSION

A numerical model of the magnetic-pumping process was constructed by alternately following the adiabatic motion of particles trapped in magnetic mirrors and solving a pitch-angle diffusion equation. The results of simulations suitably agreed with theoretical predictions for the special case of the Alfvénic model.

Our numerical techniques allowed us to manage the magnetic-pumping process when pitch-angle diffusion occurs simultaneously with the magnetic field variation. For this case we find that, as in the Alfvénic model, the mean momentum of a distribution of trapped particles, on the average, increased with time t according to

$$P(t) = P(t = 0)e^{t/\tau} \quad , \tag{23}$$

where τ is a positive constant. A resonance between the magnetic-field cycle and the pitch-angle diffusion rate gives a maximum energization efficiency for the mechanism, that is, for a certain value of the diffusion per magnetic cycle (regulated by a diffusion coefficient), the constant τ will be a minimum.

Rotating neutron stars with slightly asymmetric magnetospheres were modeled. By balancing the energy gain from the magnetic-pumping process with the energy loss by synchrotron radiation, we determined the energies, synchrotron wavelengths and power outputs of particles in the inner magnetospheres. We expect synchrotron radiation by protons, rather than by electrons, and for the parameters of our models, predict energy outputs in the range of 10^2 - 10^6 MeV per second per proton.

In order to estimate the luminosity of the neutron star, we must estimate the particle density in its magnetosphere. For an upper limit to this density we require that the plasma diamagnetic field be less than the magnetospheric field ($\beta \leq 1$ in plasma terminology), written

$$\text{particle pressure} \leq \text{magnetic pressure} \quad , \tag{24}$$

or, since the electron pressure is negligible,

$$n(\gamma - 1)mc^2 \leq \frac{B^2}{8\pi} \quad , \tag{25}$$

where m is the protonic mass and B is the magnetospheric field. This gives an upper limit for the particle number density of

$$n \leq \frac{B^2}{8\pi(\gamma - 1)mc^2} \quad . \tag{26}$$

This limit is used to estimate the magnetospheric luminosity interior to the distance r, defined

$$L(r) = \int_{r_s}^{r} P(r)n(r) \frac{4\pi r^2}{2} \, dr \tag{27}$$

where the power radiated per particle, P(r), is obtained from Equation (22), the factor of 1/2 comes from assuming half the spherical volume contains particles, and the lower limit r_s is the neutron-stellar radius. We display this luminosity L(r) for various field strengths, etc., in Figure 8. Note that since the plasma diamagnetic effect density limit (26) is independent of the angular rotation ratio Ω, and since this limit for n is several orders of magnitude smaller than the force balance limit given by (m_s = mass neutron star)

$$G \frac{m_s m}{r^2} n - \nabla\left(\frac{B^2}{8\pi}\right) - \nabla(n(\gamma - 1)mc^2) = n m \Omega^2 r \quad , \tag{28}$$

an increase in Ω by a factor of $\sqrt{10}$ will change $P(r)$ by a factor of 10 without changing $n(r)$, hence will increase the luminosity $L(r)$ by a factor of 10.

Finally we would like to point out that other losses besides synchrotron radiation (e.g., outward mass transport, collisional losses, precipitation onto the star) have not been considered in our model. All these losses are only important if the loss times associated with the processes are shorter than the energization time or radiation lifetime. Collision times are certainly much larger than the times considered here which are of the order of several rotation periods. Only strong mass transport rates, such that the plasma radial velocity is larger than the corotation speed, would reduce the efficiency of our mechanism. The effect of precipitation is difficult to estimate but the extreme smallness of the loss cone in the region where the synchrotron radiation is generated should guarantee a small loss rate.

JOSEPH E. BOROVSKY: NASA/Goddard Space Flight Center, Planetary Magnetospheres Branch, Greenbelt, MD 20771.

CHRISTOPH K. GOERTZ: Max-Planck Institut für Aeronomy, Postfach 20, D-3441 Katlenburg, Lindau 3, West Germany.

GLENN JOYCE: JAYCOR, 205 South Whiting Street, Alexandria, VA 22304.

ACKNOWLEDGMENTS

The authors wish to thank Alice Shank, John Birkbeck, and Jeana Wonderlich for their assistance. A special note of thanks to Larry Schroeder. This work was supported by the Atmospheric Science Section of the National Science Foundation and by NASA grants NSG-7632 and NGL-16-001-002.

REFERENCES

Alfvén, H. 1954, Tellus, 6, 232.

Alfvén, H., and Fälthammar, C.-G. 1963, Cosmical Electrodynamics (London: Oxford).

Borovsky, J. E. 1980, M.S. thesis, University of Iowa.

Borovsky, J. E., Goertz, C. K., and Joyce, G. 1980, submitted to J. Geophys. Res.

Goertz, C. K. 1978, J. Geophys. Res., 83, 3145.

Gurskey, H., and Schrier, E. 1975, in Neutron Stars, Black Holes, and Binary X-Ray Sources, ed. H. Gurskey and R. Ruffini (Dordrecht: D. Reidel Publishing Co.), 175.

Hinata, S., and Jackson, E. A. 1974, Ap. J., 192, 703.

Lamb, F. K., Pethick, C. J., and Pines, D. 1973, Ap. J., 184, 271.

FIGURE CAPTIONS

Figure 1. Time dependence of mean momentum of a distribution in the continuous-diffusion magnetic-pumping model.

Figure 2. Neutron star magnetospheric model: weak magnetic dipole moment, weak compression.

Figure 3. Neutron star magnetospheric model: medium magnetic dipole moment, weak compression.

Figure 4. Neutron star magnetospheric model: strong magnetic dipole moment (applicable to Crab Pulsar), weak compression.

Figure 5. Neutron star magnetospheric model: weak magnetic dipole moment, strong compression.

Figure 6. Neutron star magnetospheric model: medium magnetic dipole moment, strong compression.

Figure 7. Power radiated per proton in the synchrotron mode for various magnetospheric parameters.

Figure 8. Synchrotron luminosities of magnetospheres interior to radius r as functions of r.

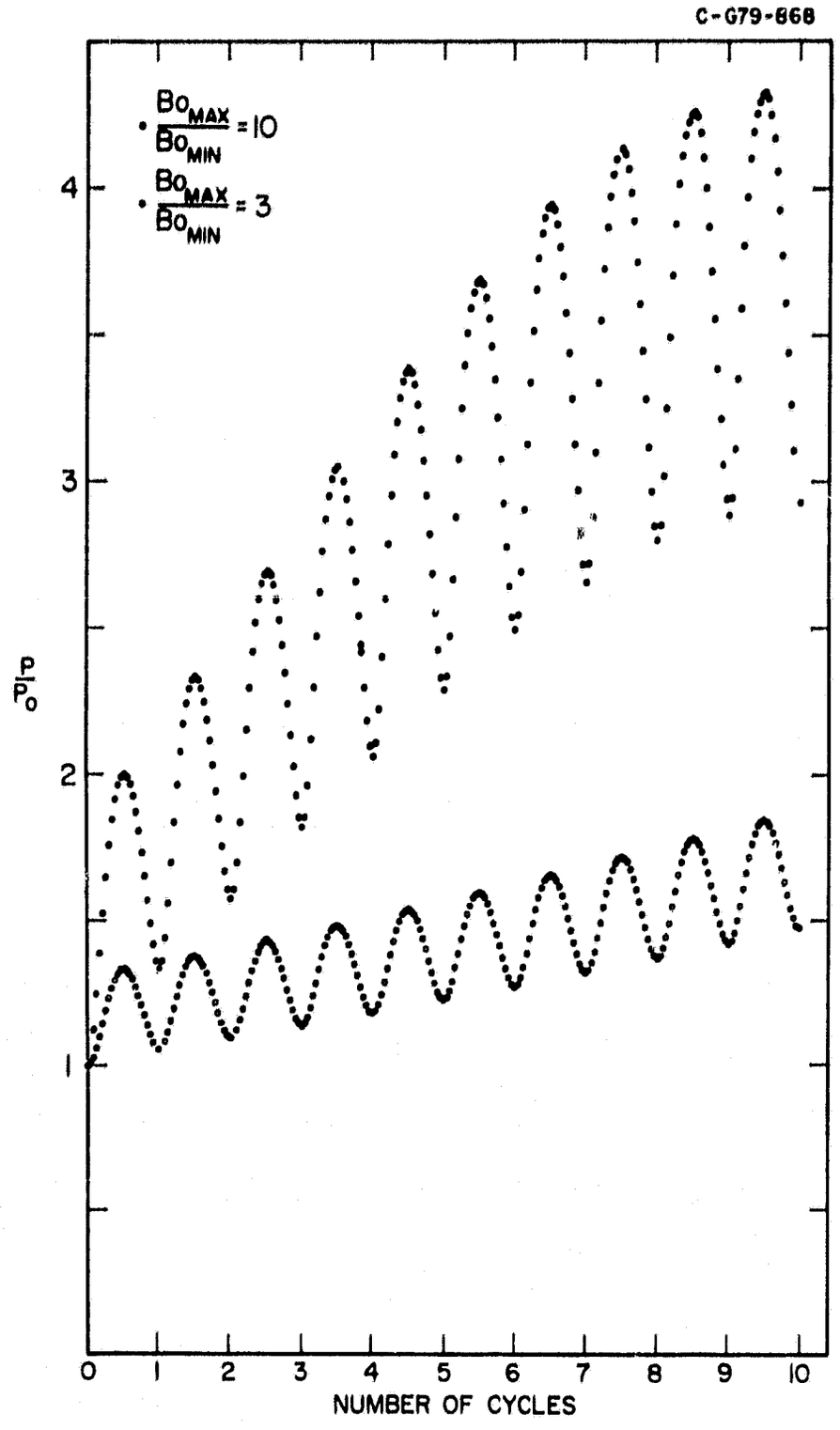
C-G79-868
$\frac{Bo_{MAX}}{Bo_{MIN}} = 10$
$\frac{Bo_{MAX}}{Bo_{MIN}} = 3$
$\frac{P}{P_o}$
1
2
3
4
0
1
2
3
4
5
6
7
8
9
10
NUMBER OF CYCLES

Figure 1

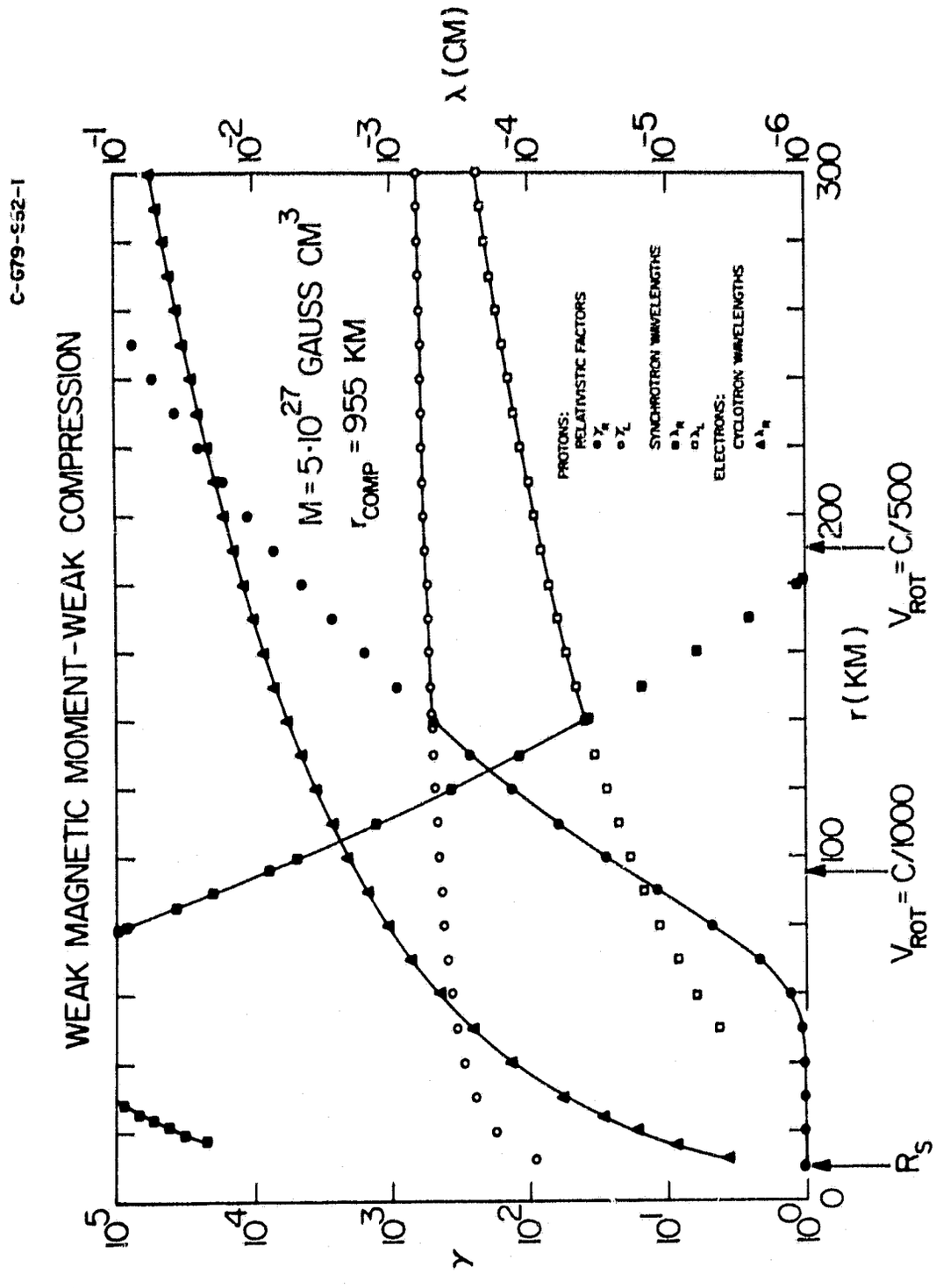
C-G79-552-1
WEAK MAGNETIC MOMENT-WEAK COMPRESSION
M = 5·10^27 GAUSS CM^3
r_COMP = 955 KM
λ (CM)
γ
r (KM)
PROTONS:
RELATIVISTIC FACTORS
SYNCHROTRON WAVELENGTHS
ELECTRONS:
CYCLOTRON WAVELENGTHS
V_ROT = C/1000
V_ROT = C/500
R_S

Figure 2

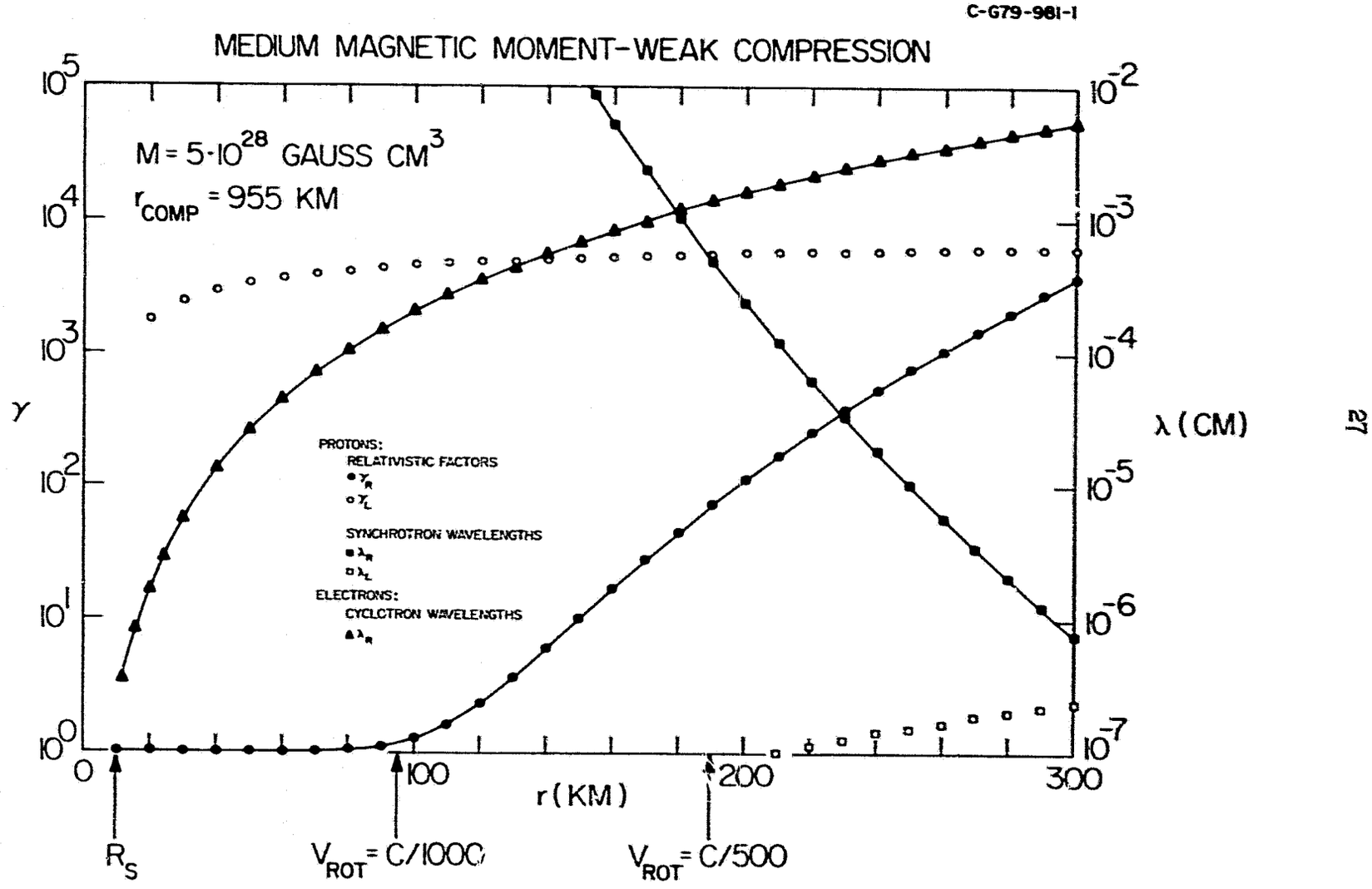
C-G79-981-1
MEDIUM MAGNETIC MOMENT-WEAK COMPRESSION
M = 5·10^28 GAUSS CM^3
r_COMP = 955 KM
γ
λ (CM)
PROTONS:
RELATIVISTIC FACTORS
SYNCHROTRON WAVELENGTHS
ELECTRONS:
CYCLOTRON WAVELENGTHS
r(KM)
R_S
V_ROT = C/1000
V_ROT = C/500

Figure 3

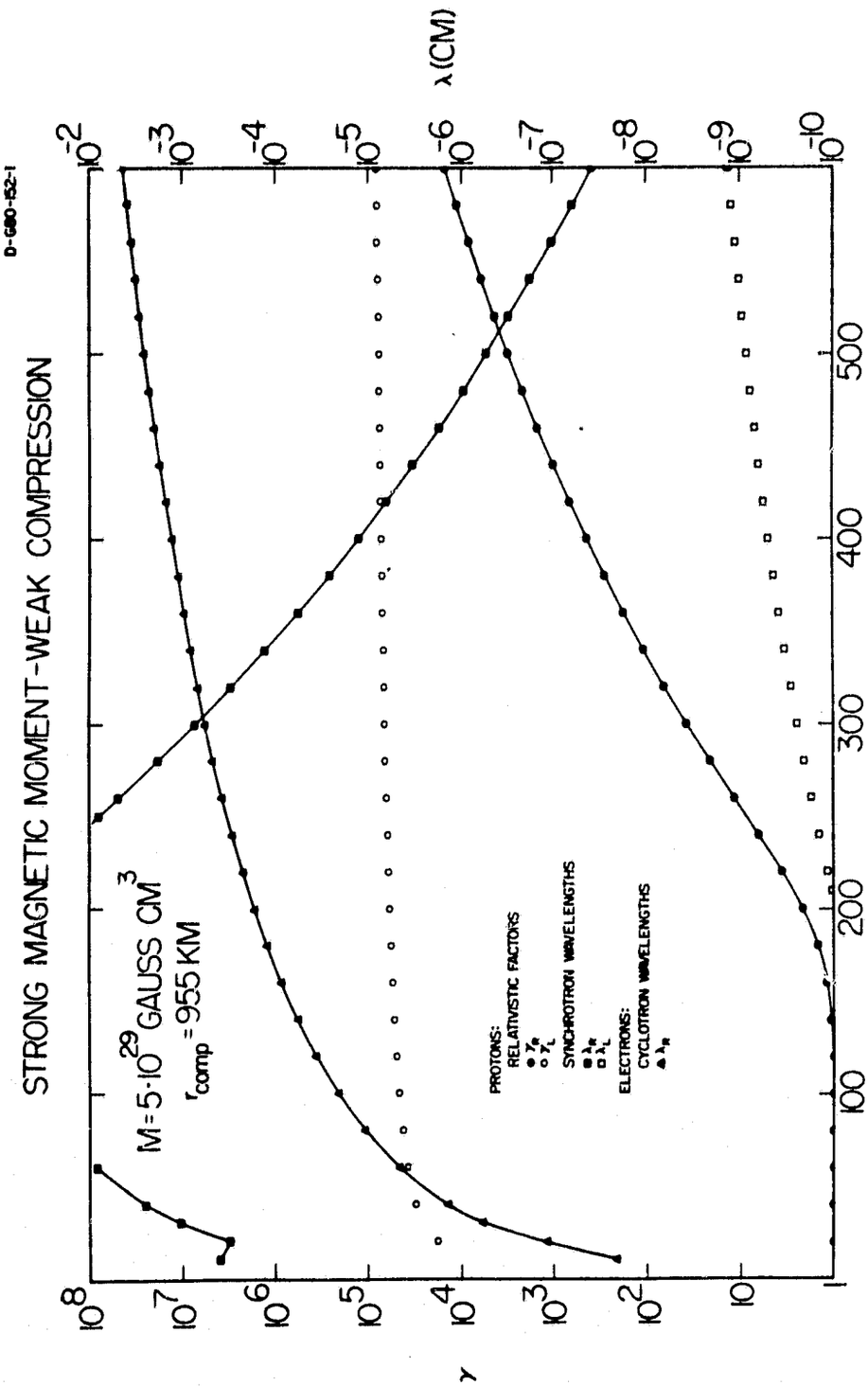
STRONG MAGNETIC MOMENT-WEAK COMPRESSION
D-680-152-1
M=5·10^29 GAUSS CM^3
r_comp = 955 KM
PROTONS:
RELATIVISTIC FACTORS
SYNCHROTRON WAVELENGTHS
ELECTRONS:
CYCLOTRON WAVELENGTHS
γ
λ(CM)
r (KM)

Figure 4

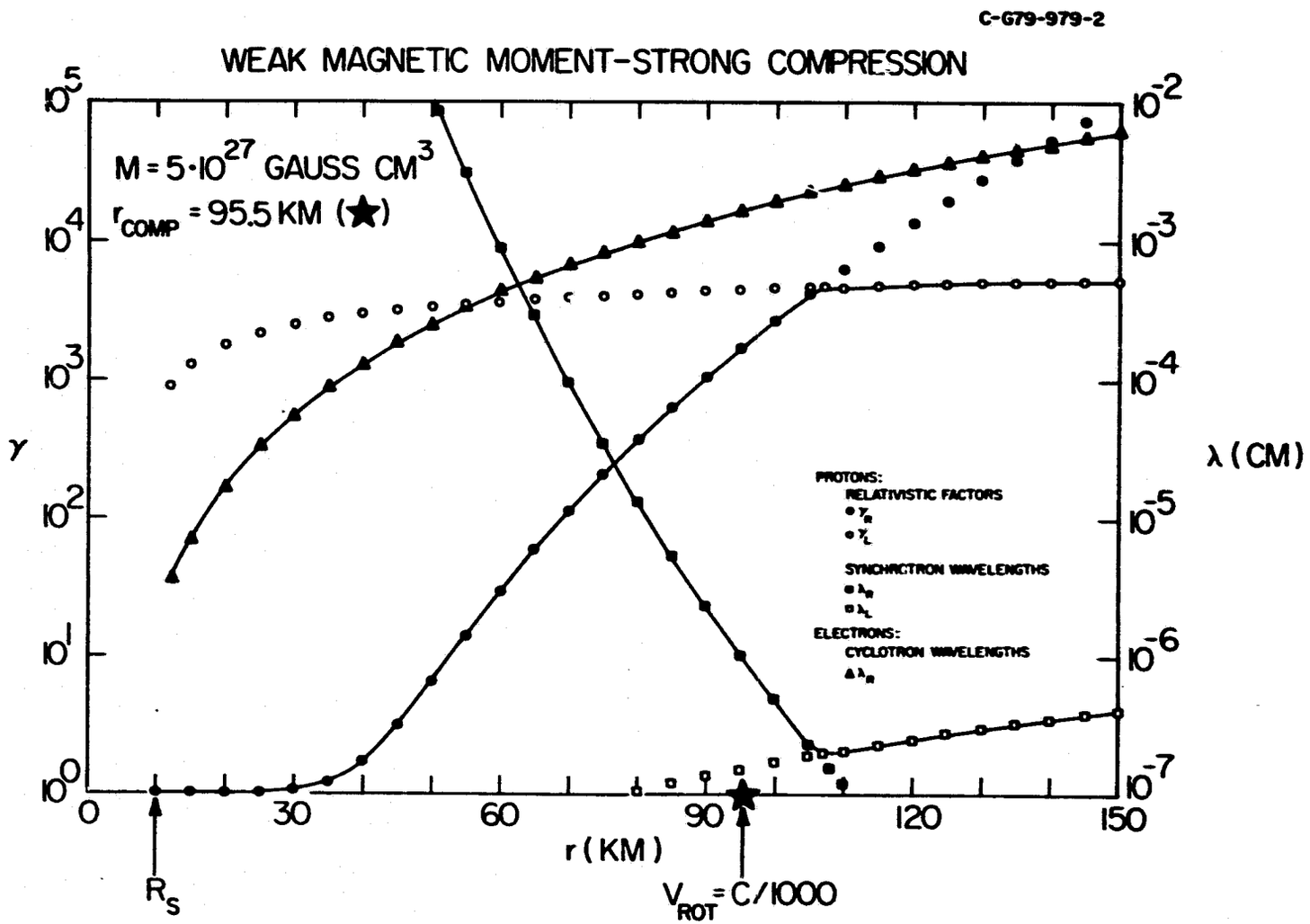
C-G79-979-2
WEAK MAGNETIC MOMENT-STRONG COMPRESSION
M = 5·10^27 GAUSS CM^3
r_COMP = 95.5 KM (★)
γ
λ (CM)
r (KM)
R_S
V_ROT = C/1000
PROTONS:
RELATIVISTIC FACTORS
SYNCHROTRON WAVELENGTHS
ELECTRONS:
CYCLOTRON WAVELENGTHS

Figure 5

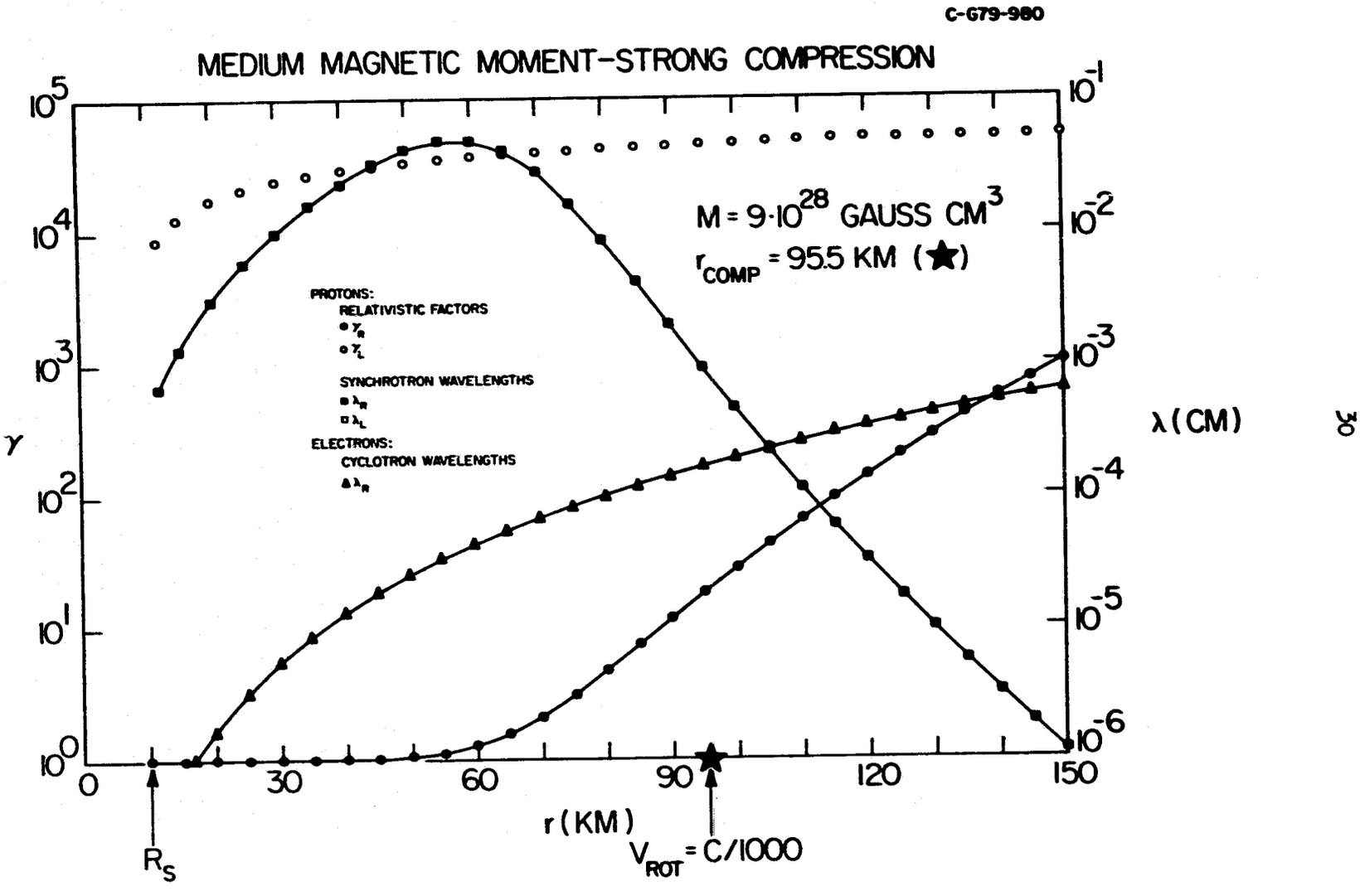
C-G79-980
MEDIUM MAGNETIC MOMENT-STRONG COMPRESSION
M = 9·10^28 GAUSS CM^3
r_COMP = 95.5 KM (★)
PROTONS:
RELATIVISTIC FACTORS
SYNCHROTRON WAVELENGTHS
ELECTRONS:
CYCLOTRON WAVELENGTHS
γ
λ (CM)
r (KM)
R_S
V_ROT = C/1000
10^5
10^4
10^3
10^2
10^1
10^0
10^-1
10^-2
10^-3
10^-4
10^-5
10^-6
0
30
60
90
120
150

Figure 6

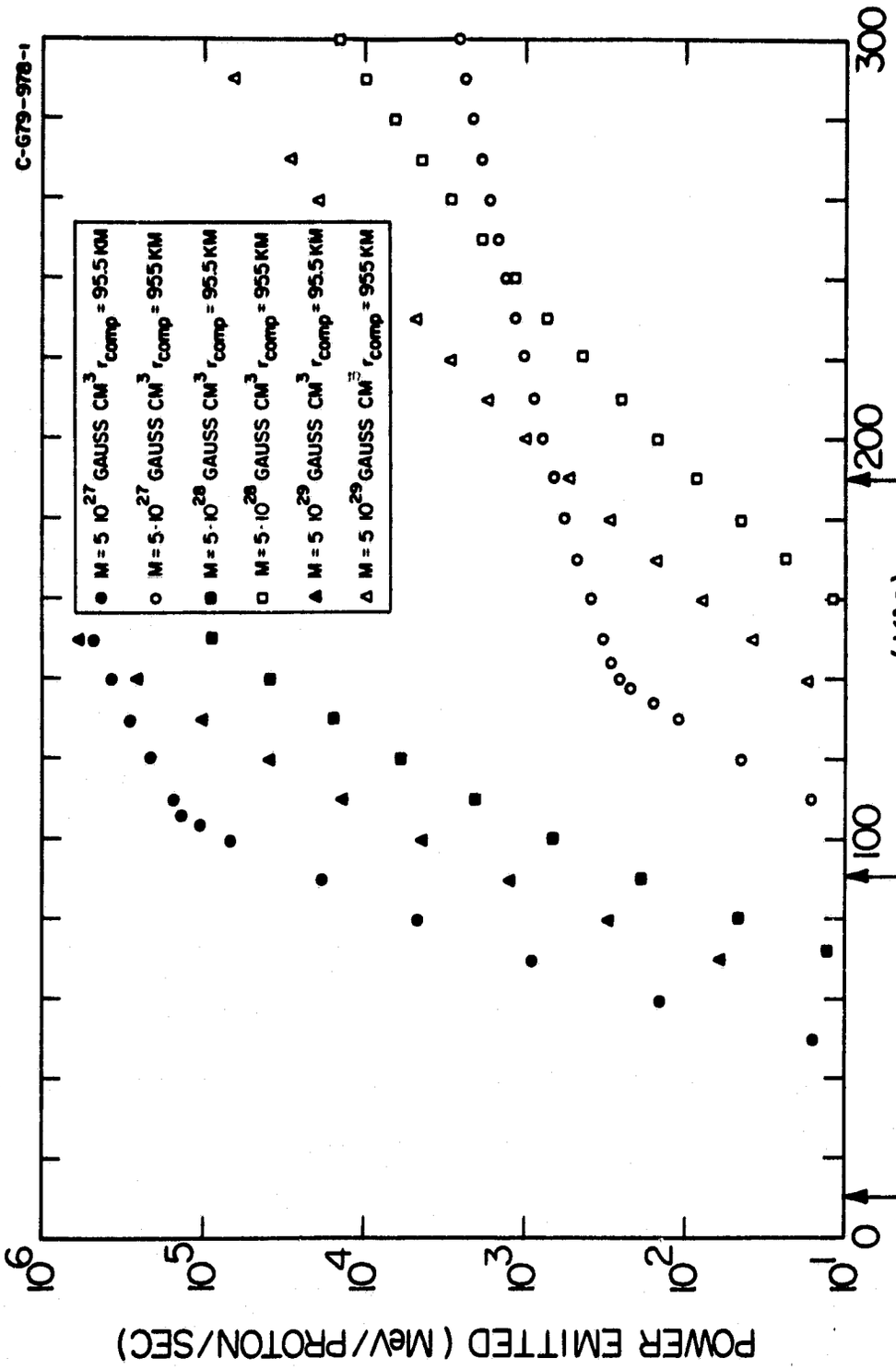
C-679-978-1
POWER EMITTED (MeV/PROTON/SEC)
r (KM)
R_S
$V_{rot} = C/1000$
$V_{rot} = C/500$
10^0
10^1
10^2
10^3
10^4
10^5
10^6
100
200
300
$M = 5 \cdot 10^{27}$ GAUSS CM^3 $r_{comp} = 95.5$ KM
$M = 5 \cdot 10^{27}$ GAUSS CM^3 $r_{comp} = 955$ KM
$M = 5 \cdot 10^{28}$ GAUSS CM^3 $r_{comp} = 95.5$ KM
$M = 5 \cdot 10^{28}$ GAUSS CM^3 $r_{comp} = 955$ KM
$M = 5 \cdot 10^{29}$ GAUSS CM^3 $r_{comp} = 95.5$ KM
$M = 5 \cdot 10^{29}$ GAUSS CM^3 $r_{comp} = 955$ KM

Figure 7

D-G80-154

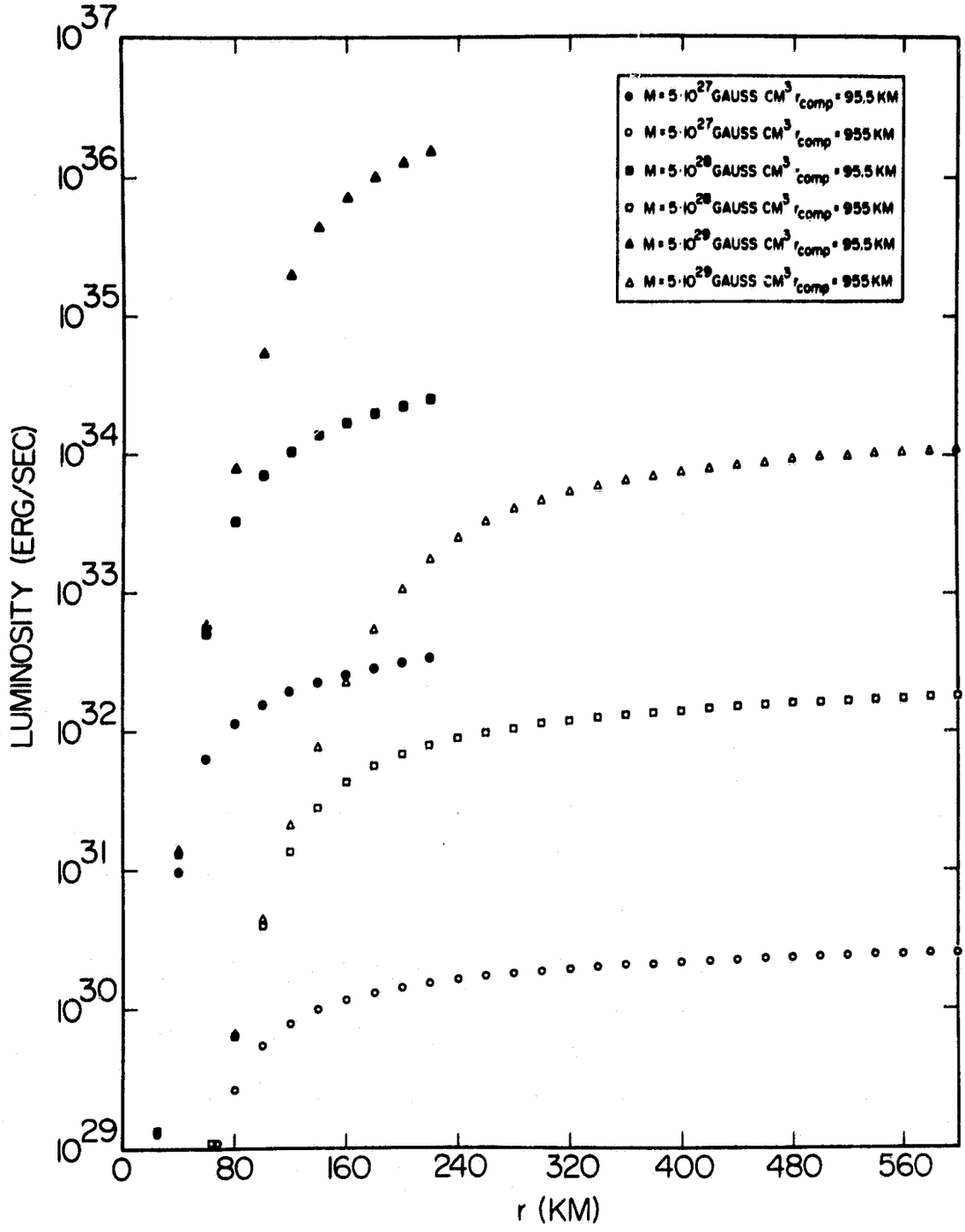

Figure 8